Mechanisms of Complete Turbulence Suppression in Turbidity Currents Driven by Mono-disperse and Bi-disperse Suspensions of Sediment

Mrugesh Shringarpure, Mariano I. Cantero and S. Balachandar

Mechanisms of Complete Turbulence Suppression in Turbidity Currents Driven by Mono-disperse and Bi-disperse Suspensions of Sediment

Mrugesh S. Shringarpure[1], Mariano I. Cantero[2] and S. Balachandar[1]

[1]Department of Mechanical and Aerospace Engineering, University of Florida, Gainesville, USA.

[2]Institute Balseiro, (CNEA-UNCu), Bariloche Atomic Center, San Carlos de Bariloche, Rio Negro, Argentina.

Abstract

Turbidity currents are submarine flows where the sediment fluid mixture (heavy current) drives along the sloping ocean floor displacing the surrounding clear fluid (light ambient). Under the influence of gravity, the suspended sediments drive the current and at the same time settle down on the ocean bed. The interplay of turbulent mixing and settling sediments leads to stable stratification of sediments in the turbidity current. In previous studies (Cantero et al. 2009b; Cantero et al., 2009a; Cantero et al., 2012a; Talling et al., 2007) it was observed that strong settling tendency (large sediment sizes) could cause complete turbulence suppression. In this study, we will analyse this process of complete turbulence suppression by means of direct numerical simulations (DNS) of turbidity currents. In wall bounded unstratified flows, it has been long established that turbulence is sustained by the process of auto-generation of near-wall hairpin like and quasi-streamwise turbulent vortical structures. It was also identified that auto-generation is possible only when the strength of the turbulent structures is greater than a threshold value (Zhou et. al., 1996). Through quadrant analysis of Reynolds stress events and visualization of turbulent vortical structures, we observe that stratification by sediments lead to damping and spatial re-distribution of turbulent vortical structures in the flow. We propose that complete turbulence suppression is brought about by a total shutdown in the auto-generation process of the existing turbulent structures in the flow. We also identify three parameters – Reynolds number (Re_τ), Richardson number (Ri_τ) and sediment settling velocity ($\widetilde{V}_z$) that quantify the process of turbulence suppression. A criterion for complete turbulence suppression is also proposed which can be defined as a critical value for $Ri_\tau \widetilde{V}_z$. This critical value is a function of Re_τ and based on simulations, experiments and field observations it appears to have a logarithmic dependence on Re_τ (Cantero *et al*. 2012). DNS of turbidity currents driven by bi-disperse suspension of sediments is also carried out and compared with the results of mono-disperse suspensions.

1. INTRODUCTION

Gravity currents are predominantly horizontal flows driven by density difference between the current and the surrounding ambient fluid. Gravity currents form an important category of fluid flows whose manifestations are abundant in geophysical, environmental and industrial processes; snow avalanches, turbidity currents, dust storms, pyroclastic flows, lava flows, leakage of poisonous gas into ambient environment, dam-breakage etc. are some examples (Simpson 1997). Gravity currents where dispersed phases like suspended sediments impose the excess density needed for its sustained propagation exhibit rich variety of physics due to the non-conservative nature of the driving agents (Allen 2001). These flows are also of great scientific interest owing to

their ability of transporting the dispersed medium. Powder snow avalanches, dust storms, pyroclastic flows, etc. are some examples of non-conservative gravity currents. Turbidity currents are their submarine counterparts where the water close to the ocean floor is rendered heavy by the excess quantity of suspended sediments which drives the heavy (water-sediment) mixture along the ocean floor displacing the surrounding light ambient water over it. Turbidity currents can be extremely energetic, erosive, travel long distances and carry large sediment loads (Pirmez & Imran 2003; Krause *et al*. 1970). Recurring occurrences of turbidity currents are known to carve out different topographies on the ocean floor. Some of the submarine canyons are a testimony to the erosive nature of these currents.

The above characteristics make turbidity currents an important submarine sediment transport mechanism. They are responsible for the organic matter from rivers to be brought deep into the ocean where the action of high pressure and temperature transform them into hydrocarbon reservoirs over geological time scales. Therefore turbidity currents are an important category of submarine flows and an improved understanding of their dynamics is essential.

Due to the non-conservative nature of suspended sediments, apart from driving the current, they are freely exchanged with the ocean floor by means of deposition due to settling and resuspension due to erosion. Furthermore, the current itself interacts with the surrounding by entraining ambient water. To understand the dynamics of the current, one needs to understand these interactions well. The nature of these interactions are governed by factors like the amount of sediment load, properties of the sediments, state of the ocean floor, ambient conditions etc. In other words, these factors determine the rheology of the flow, which in turn determines the mechanisms responsible for entrainment of sediments from the floor and to keep them in suspension. Here we will restrict our attention to dilute turbidity currents (currents driven by dilute suspension of sediments) so that flow turbulence is the sole mechanism responsible for entraining sediments and keeping them in suspension.

It is known that the settling tendency of sediments and turbulent mixing in the flow leads to a stratified turbidity current. This stratification suppresses turbulence by limiting the exchange of mass and momentum in the bed-normal direction and in extreme cases can lead to complete shutdown of turbulence. In such extreme cases, absence of turbulence leads to heavy deposition of sediments, which may result in complete cession of the flow (Talling *et al*. 2007; Cantero *et al*. 2012a). Previous research (Pantin 1979; Parker 1982) analysed dilute turbidity currents and classified them into three states based on their ability to retain sediments as depositional, self-accelerating and auto-suspension or by-pass. In the depositional state, the current is incapable of retaining sediments and progressively loses its driving potential. Such currents will eventually cease to exist. In the self-accelerating state, the current is energetic enough not only to retain sediments but to also erode even more sediments from the floor. The driving potential of such a current will progressively increase and set up a reinforcing cycle of excessive erosion and acceleration. Auto-suspension or bypass is the limiting state where the current is energetic enough so that it exactly maintains the sediment load, i.e., the driving potential is always conserved. Here we will consider continuous currents in bypass state and focus our attention on the interaction of sediments and turbulence in the body of the current[1].

In real turbidity currents the flow is highly turbulent with a large Reynolds number of $O(10^6)$ and contain sediments of various sizes (Parker 2008). The large sized sediments do not get suspended into the flow and are transported along the ocean floor as bedload. On the other hand, washload sediments are so fine that they effectively do not settle and remain well mixed in the flow. In this work we will focus on the intermediate sized sediments that settle towards the floor and can be entrained in the flow by turbulence.

Direct numerical simulations (DNS) with Reynolds numbers comparable to field scale will require extremely high resolution in space and time. At present DNS of a field scale turbidity currents is not possible even with the current state-of-the-art high-performance computers. Therefore in terms of DNS we will be restricted to low to moderate Reynolds numbers. Nevertheless, through such simulations we can gain fundamental understanding of the effects of suspended sediments on turbulence. The understanding gained from such simulations can then be extrapolated and used in various models of field scale turbidity currents.

---

[1] As opposed to fixed volume release where the head of the current is its main manifestation, the body of the current is the main manifestation of a continuous turbidity (gravity) current.

Recently, Cantero *et al*. (2009a,b) carried out DNS of continuous dilute turbidity currents by modelling them as inclined channel flow driven by the excess density imposed by mono-disperse suspensions of sediments. This mathematical model ensured that the flow remains in by pass mode and reaches statistically steady state. Cantero *et*. *al*. (2009b) demonstrated that turbulence can be completely damped when the settling velocity of sediments exceeds a certain threshold value. However, this model employed an artificial rigid top boundary that continued to generate turbulence near the rigid top boundary and diffused downwards into the flow. This influenced the turbulence suppression by stratification and affected the identification of the suppression mechanism and a clear interpretation of the results.

We have extended the previous work by Cantero *et al*. (2009b) to obtain a comprehensive understanding of the mechanism of complete turbulence suppression. In the present model of equilibrium turbidity current a stress-free top boundary is imposed, which limits turbulence generation to only the bottom boundary. This approach has allowed complete turbulence suppression to occur over the entire channel height. However, as in the previous model, ambient fluid entrainment is not considered so that the slow streamwise development of the current can be ignored.

The model presented here preserves the essential features of turbidity currents, i.e., the flow is driven by suspended sediments and stratified by their settling. From the DNS, we observed that below a threshold value of sediment settling velocity the current remained vigorously turbulent with moderate damping effects. However, even a slight increase above the threshold sediment settling velocity brings about complete turbulence suppression in the flow. This abrupt transition is intriguing. We have explored the mechanism of this transition form both statistical and mechanistic point of view in terms of how the auto-generation of turbulent vortical structures is completely disrupted above the threshold for turbidity currents driven by mono-disperse suspensions of sediments (Shringarpure *et*. *al*., (2012)). Here we will also present a simple theoretical argument to quantify the dynamics of complete turbulence suppression. Three parameters Reynolds number (Re_τ), Richardson number (Ri_τ) and sediment settling velocity (V_z) are identified that quantify the turbulence suppression mechanism. We propose that complete turbulence suppression occurs when a critical value for $Ri_\tau V_z$ is reached. Furthermore, this critical value for is $Ri_\tau V_z$ dependent on Re_τ and from limited field observations, experiments and DNS it appears to have a logarithmic dependence on Re_τ (Cantero *et*. *al*. (2012b)).

We have also extended the existing mathematical model to incorporate bi-disperse sediment suspensions. Here we will present the DNS results of turbidity currents driven by bi-disperse suspensions. These simulations show that the dynamics of complete turbulence suppression is similar to that of the mono-disperse suspensions. Furthermore, we observed that the complete turbulence suppression criterion holds for bi-disperse suspension of sediments.

2. PROBLEM FORMULATION

Here we will describe the mathematical model for currents with bi-disperse suspensions of sediments. These currents are modelled as an inclined channel flows with a slope of θ with respect to the horizontal. The flow in the channel is driven by bi-disperse suspension of sediment that drag the fluid in the streamwise direction and also settle down stratifying the flow (see Figure 1). The suspension is assumed to be dilute so that collision between sediment particles and rheology effects can be neglected, settling velocity of sediments is assumed to be independent of local concentration and Boussinesq approximation is employed. Furthermore, the problem is simplified by assuming the smaller or the fine sediment in the bi-disperse suspension to have effectively zero settling velocity or negligible settling tendency. As a consequence of this, the complete set of dimensional governing equations are as shown below.

$$\frac{\partial \mathbf{u}}{\partial t} + \mathbf{u} \cdot \nabla \mathbf{u} = -\frac{1}{\rho_w} \nabla p + \nu \nabla^2 \mathbf{u} + \left(c_f + c_c \right) R \mathbf{e}_g \qquad (1)$$

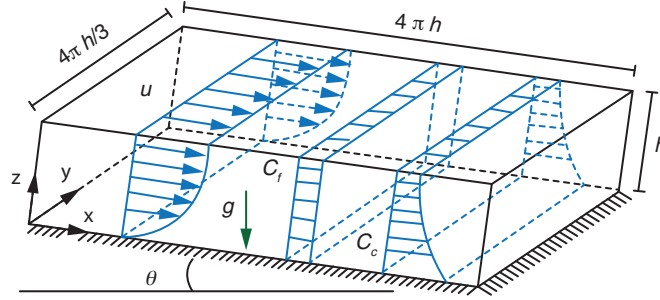$$\nabla \cdot \mathbf{u} = 0 \qquad (2)$$

Figure 1. Schematic representation of the computational domain.

$$\frac{\partial c_c}{\partial t} + \left(\mathbf{u} + \mathbf{V}_c\right)\cdot\nabla c_c = \mathcal{D}\nabla^2 c_c \tag{3}$$

The last term in (1) is the body force due to bi-disperse suspension of sediments where $R = (\rho_s - \rho_w)/\rho_w$ and c is the volumetric concentration of sediment particles. Here it is assumed that both the sediment types have approximately the same material density. $\mathbf{e}_g = \{g_x, 0, -g_z\}$ is the gravity vector in the reference frame attached to the inclined channel. Implicit in these equations is that the inertial effects of the sediments are of second order compared to the settling effects (Ferry & Balachandar 2001; Cantero *et al*. 2008a,c). Notice that the model does not contain a concentration equation for fine sediments. This is because the fine sediments have negligible settling velocity, which makes its concentration equation trivial. Sediment particles are also assumed to be non-cohesive. Sediment particles are large enough so that their Brownian motion can be ignored, but diffusivity of such large particles still exist due to the long range hydrodynamic forces mediated through the continuous phase by random fluctuations in the particle number density (Segre et al. 2001; Mucha & Brenner 2003). This diffusive term also acts as a mechanism to re-suspend sediment particles form the bed (Garcia & Parker 1993).

The channel is assumed to be periodic in the streamwise and spanwise direction. The height of the simulation domain is $L_z = h$ and its streamwise and spanwise lengths are $L_x = 4\pi h$ and $L_y = 4\pi h/3$, respectively. No-slip boundary condition is imposed on the bottom boundary (bed) and the top boundary imposes no-stress condition. For coarse sediments, the top and bottom boundary of the channel imposes zero net flux of sediments. This is achieved by enforcing the local settling flux to be exactly equal to the vertical diffusive flux of the sediments on the channel boundaries. In other words, sediments that settle down on the boundary are instantly resuspended in the flow. This condition ensures that the total sediment load in the channel is conserved and the flow can reach a statistically stationary state. The boundary conditions imposed on the computational domain can be expressed mathematically as follows

$$u = 0 \quad at \quad z = 0, \tag{4}$$

$$\frac{\partial u}{\partial z} = 0, \quad \frac{\partial v}{\partial z} = 0 \quad and \quad w = 0 \quad at \quad z = h, \tag{5}$$

$$-c_c V_{cz} = \mathcal{D}\frac{\partial c_c}{\partial z} \quad at \quad z = 0 \quad and \quad z = h. \tag{6}$$

2.1 Dimensionless equations

The mathematical model described in the previous section has a fully developed statistically stationary state. The mean flow equations obtained by averaging the momentum and concentration equations over turbulence read

$$\nu \frac{d^2 \bar{u}}{dz^2} - \frac{d}{dz}\left(\overline{u'w'}\right) + \left(\bar{c}_f + \bar{c}_c\right) R \, g_x = 0,$$
(7)

$$\frac{1}{\rho_w} \frac{d\bar{p}}{dz} + \frac{d}{dz}\left(\overline{w'^2}\right) + \left(\bar{c}_f + \bar{c}_c\right) R \, g_z = 0,$$
(8)

$$\mathcal{D} \frac{d^2 \bar{c}_c}{dz^2} - V_{cz} \frac{d\bar{c}_c}{dz} - \frac{d}{dz}\left(\overline{c_c'w'}\right) = 0.$$
(9)

Averaging is done spatially in the two homogeneous directions, i.e. streamwise and spanwise, and over time. Since there is no gravitational acceleration along the spanwise direction, the mean flow in spanwise direction is 0. Similarly mean velocity in the bed-normal direction is 0 due to continuity and no penetration condition on the channel boundaries. Also, notice that pressure appears only in (8). Integrating (7) in the bed-normal direction gives the stationary state balance between the friction on the channel boundaries and the driving force due to the buoyancy effect imposed by suspended sediments. Since the channel top boundary imposes no-stress, the driving force is balanced by friction on the bed. We can write the force balance as shown below

$$\frac{\tau_b}{\rho_w} = R \, g_x h(C_f^{(v)} + C_c^{(v)}) = R \, g_x h C^{(v)},$$
(10)

$$C_i^{(v)} = \int_0^h \bar{c}_i \, dz \quad and \quad C^{(v)} = C_f^{(v)} + C_c^{(v)}.$$
(11)

Note that the Reynolds stress term in (7) drops out, as it is exactly zero on the boundaries. From (10) we can define friction velocity as shown below

$$u_*^2 = \frac{\tau_b}{\rho_w} = R \, g_x h C^{(v)}$$
(12)

and is used as the velocity scale. Length scale is 'h' i.e. the height of the channel, time scale is h/u_*, pressure scale is $\rho_w u_*^2$ and concentration scale is $C^{(v)}$. Using these scales, governing equations (1)-(3) reduce to the following dimensionless form.

$$\frac{\partial \tilde{\mathbf{u}}}{\partial \tilde{t}} + \tilde{\mathbf{u}} \cdot \widetilde{\nabla}\tilde{\mathbf{u}} = -\widetilde{\nabla}\tilde{p} + \frac{1}{Re_\tau}\widetilde{\nabla}^2\tilde{\mathbf{u}} + \left(\tilde{c}_f + \tilde{c}_c\right)\mathbf{e}$$
(13)

$$\widetilde{\nabla} \cdot \tilde{\mathbf{u}} = 0$$
(14)

$$\frac{\partial \tilde{c}_c}{\partial \tilde{t}} + \left(\tilde{\mathbf{u}} + \widetilde{\mathbf{V}}_c\right) \cdot \widetilde{\nabla}\tilde{c}_c = \frac{1}{Re_\tau Sc}\widetilde{\nabla}^2\tilde{c}_c$$
(15)

Here $\mathbf{e} = \{1, 0, -1/\tan\theta\}$ is the dimensionless gravity vector. Reynolds number (Re_τ) and Schmidt number (Sc) are the two dimensionless parameters governing the flow and their forms are as shown here

$$Re_\tau = \frac{u_* h}{\nu} \quad and \quad Sc = \frac{\nu}{\mathcal{D}}$$

The total volumetric sediment concentration of the individual sediment types can be reduced using the concentration scale as shown

$$\gamma_c = \frac{C_c^{(v)}}{C^{(v)}} \quad \text{and} \quad \gamma_f = \frac{C_f^{(v)}}{C^{(v)}} \quad \text{so that} \quad \gamma_c + \gamma_f = 1 \tag{16}$$

In summary, the above bi-disperse formulation is a 5 parameter problem where the 5 parameters are Re_τ, Sc, θ, $\tilde{V}_c$ and γ_f (since $\tilde{V}_f \approx 0$ and $\gamma_c = 1 - \gamma_f$).

2.2 Selecting appropriate values for the parameters

Typically the inclination of the continental slope on the ocean floor ranges from 1° to 10°(Pinet, 2006), hence we fix the slope of the channel at $\theta = 5°$ in all the simulations (this gives $(\tan\theta)^{-1} = 11.43$). It is reasonable for a field turbidity current to grow to a height of $h = 20\ m$ and to be driven by a mean volume concentration $\bar{C}^{(v)} = 0.005$ of sand particles in water ($R = 1.65$ and $\nu = 10^{-6}\ m^2 s^{-1}$). Under these conditions, the definition in (12) gives $u_* = 0.38\ ms^{-1}$. Furthermore, such a turbidity current will be composed of sediment particles whose diameter ranges from 70 μm and 120 μm and their corresponding terminal settling velocities will range from $V = 0.004\ ms^{-1}$ and $0.01\ ms^{-1}$ (Parker, 2008). This range, in terms of its dimensionless form will be $\tilde{V}_z = 1 \cdot 10^{-2}$ to $\tilde{V}_z = 2.6 \cdot 10^{-2}$. The corresponding Reynolds number $Re_\tau = 7.5 \cdot 10^6$ of the field scale current is too large and therefore cannot be studied with DNS. The present simulations employ $Re_\tau = 180$ which results in mature turbulent flow and is helpful in extracting the important interactions between the suspended sediments and turbulence. Following Mucha & Brenner (2003) and Segre $et\ al.$, (2001) a rough approximation for sediment diffusivity can be $\approx 10\ a\ V$, where a is the radius of the sediment particles. Thus, for the above example, sediment diffusivity is approximately the same order of kinematic viscosity of water. Generally sediment diffusivity will depend on the local sediment concentration, concentration gradient and shear stress, but we suppress such dependencies in our present model. Based on the findings of Necker $et\ al$. (2005) and Cantero $et\ al$. (2008b) that the simulation results of turbidity currents are insensitive to the precise values of Sc as long as it is of O(1). Therefore the present simulations employ $Sc = 1$. In case of bi-disperse sediment suspensions, there are two additional parameters that need to be specified, i.e. V_c and γ_f. Since fine sediments have nearly negligible settling velocity, they will not impose any stratification on the current and conceptually γ_f is equivalent to a uniform pressure gradient acting on the flow. In other words, coarse sediments are solely responsible for inducing turbulence damping effects. This bi-disperse problem will be interesting and non-trivial only when coarse sediments are big enough ($V_c > V_{c,critical}$) to cause complete turbulence suppression. In other words, for a given size of coarse sediment there should exists a critical composition of the bi-disperse suspension so that even a small increase in the amount of coarse sediments (at the expense of fine sediments) will cause complete turbulence suppression. Table 1 shows the list of mono-disperse cases studied and Table 2 shows the list of bi-disperse cases.

Table 1. List of simulations. V_z is the dimensionless settling velocity of the sediments. $\tilde{u}_b$ is the bulk velocity of the flow. Re_b is the Reynolds number based on bulk velocity. $\bar{\bar{c}}_b$ and $\bar{\bar{c}}_t$ are the dimensionless mean volume concentration of sediments at the bed and the top boundary. B-1 and B-2 are two simulations where the top boundary was no slip

Case	$\tilde{V}$	$\tilde{u}_b$	Re_b	$\bar{\bar{c}}_b$	$\bar{\bar{c}}_t$
0	0.0	15.52	2794	1.00	1.00
1	0.01	16.13	2903	1.22	0.82
2	0.02	17.09	3076	1.55	0.58
3	0.026	18.33	3300	1.93	0.42
4	0.0265	27.32	4900	4.78	0.043
B-l	0.02125	17.48	3146	2.63	0.52
B-2	0.023	18.04	3247	4.45	0.43

Table 2. List of simulations: γ_f refers to the volume fraction of fine sediments in the mixture and $\gamma_c = 1-\gamma_f$ is the volume fraction of coarse sediments. $\bar{\bar{\tilde{u}}}_b$ is the bulk streamwise velocity, $\tilde{u}_t$ is the maximum mean streamwise velocity, $\bar{\tilde{c}}_b + \gamma_f$ and $\bar{\tilde{c}}_b + \gamma_f$ are the total sediment concentration of sediments at the bed and the top boundary of the channel, respectively. The abbreviation CTS stands for complete turbulence suppression.

Case	$\tilde{V}_c$	γ_f	γ_c	$\tilde{u}_b$	$\bar{\bar{\tilde{u}}}_t$	$\tilde{c}_{cb} + \gamma_f$	$\tilde{c}_{ct} + \gamma_f$	State
0A	0.0275	1.00	0.00	15.52	18.12	1.00	1.00	Turbulent
1A	0.0275	0.75	0.25	15.91	18.96	1.167	0.90	Turbulent
2A	0.0275	0.30	0.70	17.19	21.07	1.572	0.644	Turbulent
3A	0.0275	0.04	0.96	18.41	22.91	1.951	0.415	Turbulent
0B	0.035	1.00	0.00	15.52	18.12	1.00	1.00	Turbulent
1B	0.035	0.75	0.25	16.06	19.22	1.232	0.881	Turbulent
2B	0.035	0.30	0.70	17.78	22.28	1.880	0.546	Turbulent
3B	0.035	0.24	0.76	18.44	22.90	2.027	0.4877	Turbulent
4B	0.035	0.235	0.765	30.63	39.96	5.036	0.244	CTS

3. NUMERICAL SCHEME

We solve the dimensionless governing equations (13)-(15) using a de-aliased pseudo-spectral code (Canuto et al. 1988). Fourier expansions in the tangential direction to the bed ($\tilde{x}, \tilde{y}$) and by Chebyshev expansions in the bed-normal direction ($\tilde{z}$) are used to approximate the flow variables. Momentum equation along with the incompressibility criteria is solved by a splitting method. We use the low-storage mixed third order Runge-Kutta and Crank-Nicolson scheme is used for temporal discretization of advection and diffusion terms. This scheme is carried out in three stages with pressure correction at the end of each stage. Refer to Cortese & Balachandar (1995) for complete details on the implementation of the scheme. The grid resolution of (N_x, N_y, N_z) = (96,96,97) is used and it is found to be sufficient for the Reynolds number selected in this study (Cantero et al. 2009a; Cantero et al. 2009b).

4. RESULTS AND DISCUSSION

Here we will first briefly describe the results of DNS of turbidity currents driven by mono-disperse suspensions of sediments. Previous research has highlighted the existence of a critical settling velocity beyond which complete turbulence suppression occurs (Cantero et al. 2009a; Cantero et al. 2009b). The underlying mechanisms responsible for complete turbulence suppression were explored through DNS of the mathematical model proposed in the previous section. Table 1 lists some of the simulations analysed in this work. Four different cases of stratified flows are considered. Cases 1 to 4 correspond to simulations where the settling velocity of sediments is increased from $\tilde{V}_s = 1\cdot10^{-2}$ to $\tilde{V}_s = 2.65\cdot10^{-2}$. Case 0, with $\tilde{V}_s$, is the reference case, since its solution corresponds to unstratified turbulent channel flow driven by a uniform body force.

4.1 Turbulence statistics

The mean concentration profiles of selected cases given in Table 1 are shown in Figure 2(a). As the settling velocity of sediments increases, the resulting concentration profile increasingly deviates from the reference profile of case 0. The mean concentration profile generated due to settling sediments results in driving force, represented by the streamwise component of the body force (see the last term on the right hand side of (13)), skewed towards the bed. On the other hand, the stable stratification induced by concentration gradients tends to dampen turbulence and this effect is captured by the bed-normal component of the body force (see the last term on the right hand side of (13)).

　　Figure 2(a) shows a clear change of regime from case 3 to case 4. While case 3 shows a well-mixed concentration profile, the concentration profile for case 4 is nearly zero in the top part of the channel and presents large values in the near-bed region. Corresponding mean velocity profiles are shown in Figure 2(b), and they also show a clear change of regime from case 3 to case 4. While the
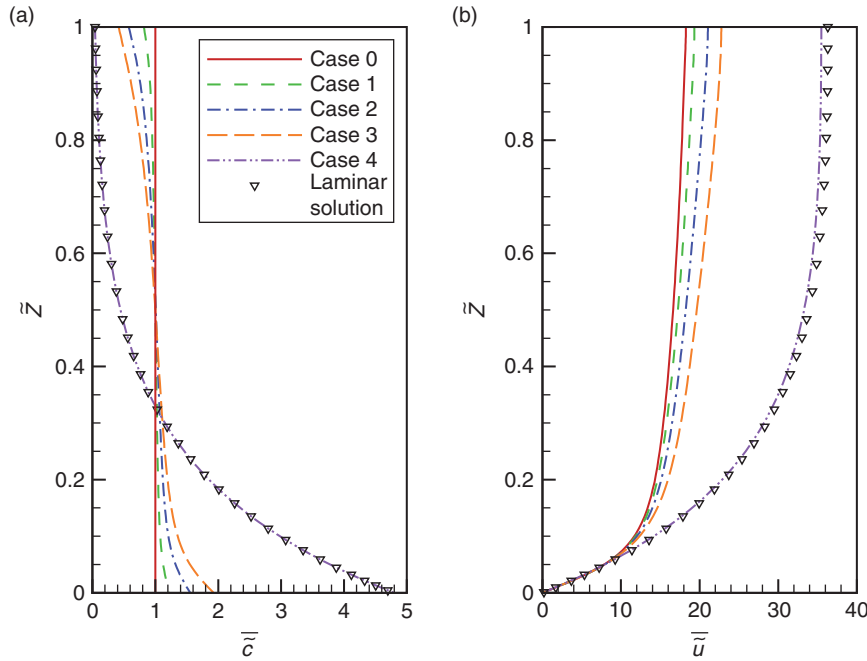
Figure 2. (a) Mean concentration profiles. (b) Mean velocity profiles. All the cases belong to turbidity currents driven by mono-disperse suspensions. Refer to table 1 for complete details.

velocity profile for case 3 shows a small deviation from the turbulent velocity profile of case 0, the velocity profile for case 4 shows less mixing and resembles a laminar profile.

Another important statistic of interest is the Reynolds flux or turbulent mixing in the flow. The balance between the settling flux of sediments $\widetilde{V}_z \overline{\widetilde{c}}_s$ and the turbulent flux of sediments $\overline{\widetilde{w}' \widetilde{c}'}$ can be obtained from (9) as

$$\widetilde{V}_z \overline{\widetilde{c}} = \overline{\widetilde{w}' \widetilde{c}} - \frac{1}{Re_\tau Sc} \frac{d\overline{\widetilde{c}}}{d\widetilde{z}} \tag{17}$$

In order to keep the sediments well mixed in the flow $\partial \overline{\widetilde{c}} / \partial \overline{\widetilde{z}} \approx 0$, there must be a proportionate increase in the turbulent flux as the settling velocity of sediments increases. The relative importance of turbulent flux of sediments can be seen in Figure 3(a), which shows the variation in the ratio of turbulent flux to settling flux in the bed-normal direction. From Figure 3(a) it is evident that the increase in turbulent flux is not proportionate for all the cases shown. This ratio shows a decreasing trend with increasing settling velocity of sediments, but the decrease is not very sensitive for cases 1 to 3. Also, the decrease is not uniform throughout the channel, it is more pronounced near the top boundary than near the bed. This asymmetry is due to reduction of turbulent transport from near the bed, where turbulence production occurs, to the upper part of the channel. For case 4 the turbulent flux of sediments is zero, which confirms that total turbulence suppression has indeed occurred.

Figure 3(b) shows profiles of the Reynolds stress $\overline{\widetilde{u}' \widetilde{w}'}$ For cases 1 to 3 the small reduction in Reynolds stress with increase in the settling velocity of sediments suggests that the effect of stratification is weak. However, with further increase in settling velocity of sediments above the critical value, a dramatic shut-off is seen in the Reynolds stress.

Before we delve into other higher order turbulence statistics, lets look at the stratification effect on simple turbulence models like eddy diffusivity. An important advantage of DNS is to be able to aid development of more accurate turbulence models for such flows. From the DNS data we can compute eddy viscosity in the channel as shown here
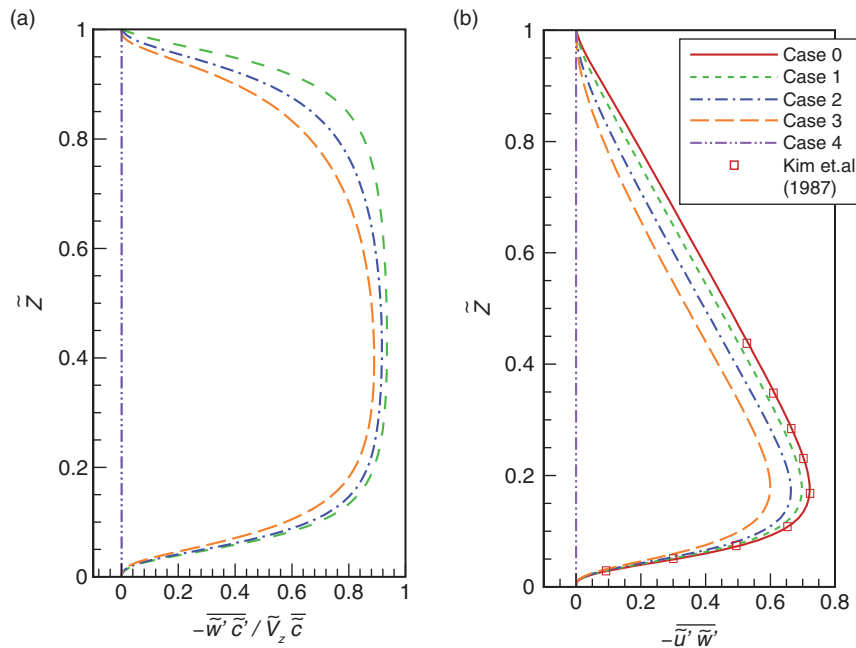
Figure 3. (a) Ratio of sediment turbulent flux to settling flux. (b) Reynolds stress profiles for cases listed in table 1.

$$\frac{v_T}{v} = \frac{-\overline{\tilde{u}'\tilde{w}'}}{1/Re_\tau \; d\overline{\tilde{u}}/d\tilde{z}} \qquad (18)$$

Figure 4(a) shows the profile of eddy viscosity in the channel as the settling velocity of the suspended sediment particles is increased from case 0 to case 3. For case 0 the eddy viscosity is nearly symmetric about $\tilde{z} \sim 0.5$. With increase in the sediment settling velocity, the profiles get damped and skewed towards the bottom. Clearly, the stratification effect alters the nature of eddy viscosity. Also shown in the figure by symbols is the eddy viscosity model $v_T = \kappa u_* z(1 - z)$. Here κ is the von Karman constant. For turbulence-stratified cases 1 to 3 a modified value of von Karman constant is used. This value is such that it gives a good log law fit for the mean streamwise velocity profile. Values taken by κ are provided in the figure caption. As expected this model does a fair job away from the bottom wall for the pure channel flow case (case 0). From the figure it is clear that stratification modifies the turbulence associated with a pure channel flow substantially. Using a modified value for κ in the eddy viscosity model may give a reasonable approximation of the mean flow.

Turbulence models are also needed to obtain the concentration profile in the channel. Typically turbulent fluxes arising out of the concentration equation have been approximated by the eddy diffusivity assumption ($D_T = \beta\kappa u_* z(1 - z)$ where β is a proportionality constant). As seen earlier, the stratification effect of suspended sediments inhibits wall normal mixing of momentum and mass. Figure 4(b) shows the eddy diffusivity profiles obtained from the DNS data (profiles represented by lines). We can write eddy diffusivity as

$$\frac{D_T}{v} = \frac{-\overline{\tilde{w}'\tilde{c}'}}{1/Re_\tau \; d\overline{\tilde{c}}/d\tilde{z}} \qquad (19)$$

Furthermore, the eddy diffusivity can be approximated using the modified κ value obtained from the eddy viscosity profiles. These approximations are also represented in Figure 4(b) by symbols.
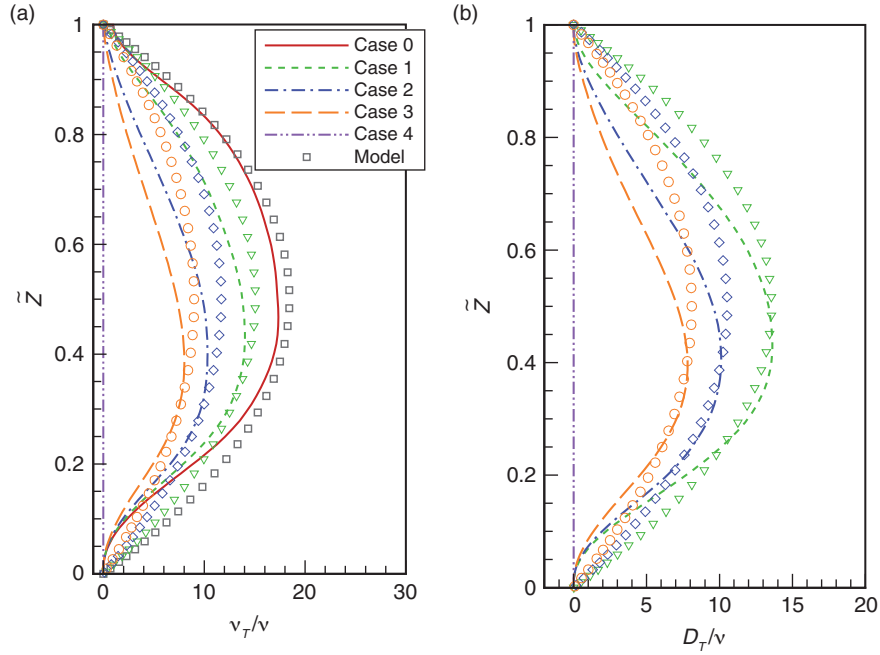
Figure 4. (a) Eddy viscosity and (b) Eddy diffusivity profiles inside the channel under varying stratification imposed by mono-disperse suspension of sediments. Lines represent profiles computed from the simulation. Symbols represent the corresponding eddy viscosity or eddy diffusivity model. Modified von Karman constant for case 1 is $\kappa_{mod} = 0.335$, for case 2 is $\kappa_{mod} = 0.26$ and for case 3 is $\kappa_{mod} = 0.20$. The proportionality constant $\beta = 0.90$ for all cases.

It is evident that a parabolic profile for eddy diffusivity or viscosity will over predict the amount of turbulence mixing away from the bottom wall considerably.

4.1.1 Turbulent kinetic energy balance

From the previous analysis it is clear that beyond the critical settling velocity there is abrupt shutdown of turbulence in the flow. Let us now look at some of the important terms in the turbulent kinetic energy (TKE) equation to understand the effect of stratification on them. Following is the TKE equation for statistically stationary flow field in its dimensionless form.

$$\tilde{p} - \tilde{\in} + \tilde{D} + \tilde{T} - \frac{\overline{d\tilde{w}'\tilde{p}'}}{d\tilde{z}} = -\tilde{F}_\mathrm{X} + \mathrm{Ri}_\tau \tilde{F}_z. \tag{20}$$

where $\widetilde{P}$ is TKE production, $\tilde{\in}$ is TKE dissipation, $\tilde{k}$ is TKE, $\widetilde{D}$ is diffusion of TKE and $\tilde{T}$ is transport of TKE by velocity fluctuations.

$$\tilde{p} = -\overline{\tilde{u}_i'\tilde{u}_j'}\frac{\partial \overline{\tilde{u}}_i}{\partial \tilde{x}_j}, \tilde{\in} = \frac{1}{Re_\tau}\overline{\frac{\partial \tilde{u}_i'}{\partial \tilde{x}_j}\frac{\partial \tilde{u}_i'}{\partial \tilde{x}_j}}, \tilde{k} = \frac{\overline{\tilde{u}_i'\tilde{u}_i'}}{2}, \tilde{D} = \frac{1}{Re_\tau}\frac{d^2\tilde{k}}{d\tilde{z}^2}, \tilde{T} = -\frac{d\,\overline{\tilde{w}'\tilde{k}}}{d\tilde{z}} \text{ and } \tilde{F}_i = \overline{\tilde{u}_i'\tilde{c}'}.$$

In the above equation, terms on the right hand side arise out of the buoyancy terms that were present in the momentum equations. These terms can be interpreted as the amount of TKE spent by the flow locally to keep the sediment particles in suspension. The terms in the square brackets are the TKE transport terms due to various mechanisms like advection due to velocity fluctuations, transport by pressure fluctuations and viscous transport or diffusion. Figure 5 shows the TKE profiles. As seen before, for suspensions containing sediments that have subcritical settling velocity
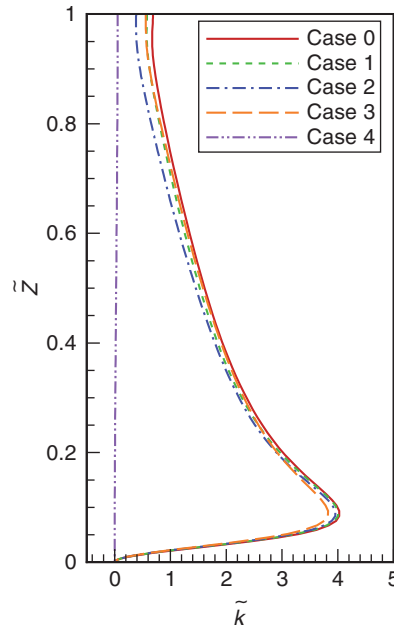
Figure 5. Profiles of turbulent kinetic energy associated with different mono-disperse suspensions. Refer to Table 1 for complete details.
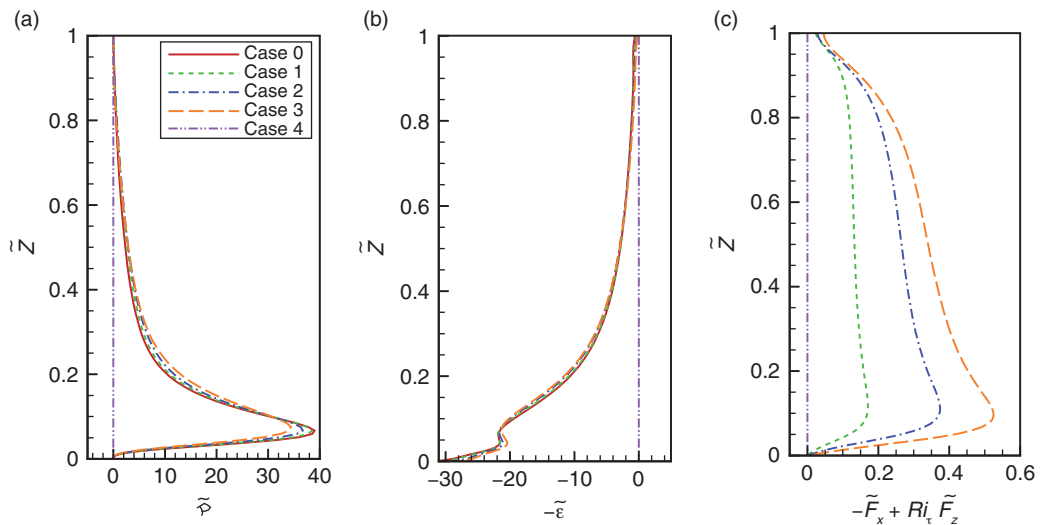

Figure 6. Profiles of (a) TKE production, (b) dissipation and (c) damping associated with different mono-disperse suspensions. Refer to Table 1 for complete details.

(case 1 to case 3) the stratification effect results in only weak damping of TKE. However, as soon as the settling velocity of sediment particles is increased beyond the critical value (case 4) it results in complete shutdown of TKE.

Similar trends are seen for TKE production and TKE dissipation terms (see Figure 6(a) and 6(b)). TKE production profiles for case 1 to 3 show weak damping. About 10 % damping is observed for TKE production peak for case 3. However, there is sudden shutdown of turbulence at case 4 and the TKE production is exactly zero throughout the channel height. This abrupt and total turbulence suppression is intriguing as it occurs due to slight increase in the sediment settling velocity beyond case 3. On the other hand, TKE damping (the terms on the right hand side of (20)) is observed to increase proportionately with the settling velocity of sediment particles (see Figure 6(c)). But interestingly, the TKE damping terms are only a small fraction

of TKE production, especially in the region of TKE production peak. This suggests that TKE damping terms have a strong influence on the flow and even small quantities can potentially lead to complete turbulence suppression.

We now probe into the effect of stratification on the transport terms in the TKE equation. Figure 7 (a), (b) and (c) presents the TKE diffusion ($\widetilde{D}$), TKE transport due to velocity perturbations $\widetilde{T}$ and TKE transport due to pressure perturbations for the mono-disperse suspensions (see (20)). As expected TKE diffusion process is active and strong very close to the bottom wall. Sufficiently away from the boundary TKE is predominantly transported due to turbulent convection (velocity perturbations) and pressure transport term. Furthermore, the TKE diffusion process is nearly independent of the stratification effect. All the profiles (case 0 to case 3) are nearly on top of each other. This is expected, as the stratification effect will not interfere with the diffusion mechanism, which is only depends on the Reynolds number of the flow. In the TKE balance the deficit between production and dissipation is balanced by the transport terms and the damping terms. Figure 7(b) shows the profiles of TKE transport due to wall normal velocity fluctuations. As the settling velocity of sediment particles is increased from case 0 to case 3, the increased stratification is responsible for inhibiting the transport of TKE from the location of TKE production peak into the bulk flow. While the transport towards the bottom wall is seen to increase with settling velocity.

These results lead to the viewpoint that there exists a critical value for settling velocity of sediments and even a small increase beyond this value will cause a sudden change in the flow regime.

4.2 Reynolds stress events

The mechanism by which turbulence is sustained in a wall-bounded flow even when the wall is smooth has been an active area of research (Brooke *et al*. 1993; Bernard *et al*. 1993; Zhou *et al*. 1996; Zhou *et al*. 1999). One of the proposed mechanisms relies on the auto-generation of vortical structures and their arrangement as streamwise aligned packets (Zhou *et al*. 1996; Zhou *et al*. 1999). These hairpin and other quasi-streamwise vortices in a turbulent wall layer generate secondary, tertiary and additional vortical structures over time and sustain turbulence. It is also shown that only when the amplitude (strength) of the vortical structures is above a certain threshold they possess the ability of auto-generation. The implication is that if the strength of the vortical structures falls below a certain threshold they lose their ability to auto-generate and thus fail to sustain turbulence.

We pursue the arguments presented above to explore the effect of suspended sediments on the vortical structures in the flow. For the mono-disperse cases considered, a quadrant analysis of
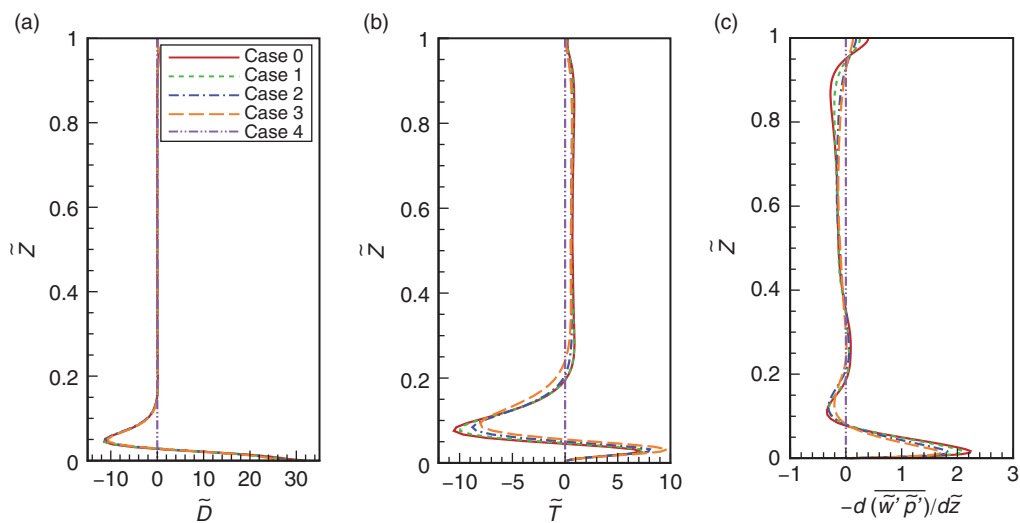

Figure 7. Profiles of (a) TKE diffusion, (b) TKE transport due to wall normal velocity fluctuations and (c) TKE transport due to pressure perturbations associated with different mono-disperse suspensions. Refer to Table 1 for complete details.

the streamwise and bed-normal velocity fluctuations is performed to obtain a statistical picture of the Reynolds stress distribution. By analysing the Reynolds stress events, we obtain qualitative understanding of the behaviour of vortical structures in an environment of increasing stable stratification. From the $\tilde{u}' - \tilde{w}'$ scatter plot, the probability $P(\xi) = \Pr\{\tilde{u}'\tilde{w}'\}$ that the local instantaneous Reynolds stress takes a value ξ is computed. Traditionally the $\tilde{u}' - \tilde{w}'$ scatter plot is divided into four quadrants, of which quadrant– 2 (Q2) and quadrant– 4 (Q4) contribute to negative Reynolds stress and have been recognized to be the most significant. Q2 events correspond to quasi-streamwise and hairpin vortices in the flow, which are responsible for sustaining turbulence. Therefore negative Reynolds stress contributions from Q2 and Q4 events are separated in computing the probability. Q2 events cause low momentum fluid present close to the bed to be ejected into the bulk flow and hence are an ideal mechanism for vertical mixing or to resuspend settling sediments.

Figure 8(a) shows $|\xi P(\xi)|$ versus Reynolds stress value (ξ) for the second quadrant events at $\tilde{z}^+ = 18$ for cases 0 and 3. Results for other bed-normal locations are similar and therefore not shown. The stress at which $|\xi P(\xi)|$ reaches a peak value can be interpreted as the turbulent event that makes the largest contribution to the time and horizontal averaged mean Reynolds stress. Lets denote this Reynolds stress value as ξ_m. For case 0, $\xi_m = -1.26$ and the corresponding value of the turbulent event (fluctuating velocity) is $\tilde{u}'_m = (-2.42, 0, 0.521)$. Furthermore, the conditionally averaged flow field (conditional eddy) corresponding to this Reynolds stress event is a hairpin vortex (Adrian 1994). So the question of turbulence sustainment can be posed in terms of the ability for this Reynolds stress maximizing hairpin vortex to produce and populate the subsequent generations of vortical structures (Adrian 2007). In the clear fluid case (case 0) the turbulent vortical structures are self-sustaining and the turbulence generation continues uninterrupted.

For case 3 the peak contribution to Reynolds stress occurs at a lower value of $\xi_m = -0.68$ and the corresponding turbulent velocity event is $\tilde{u}'_m = (-2.10, 0, 0.323)$. We can see from the Figure 3(b) that the mean Reynolds stress at $\tilde{z}^+ = 18$ (peak location) decreases by only about 17% from
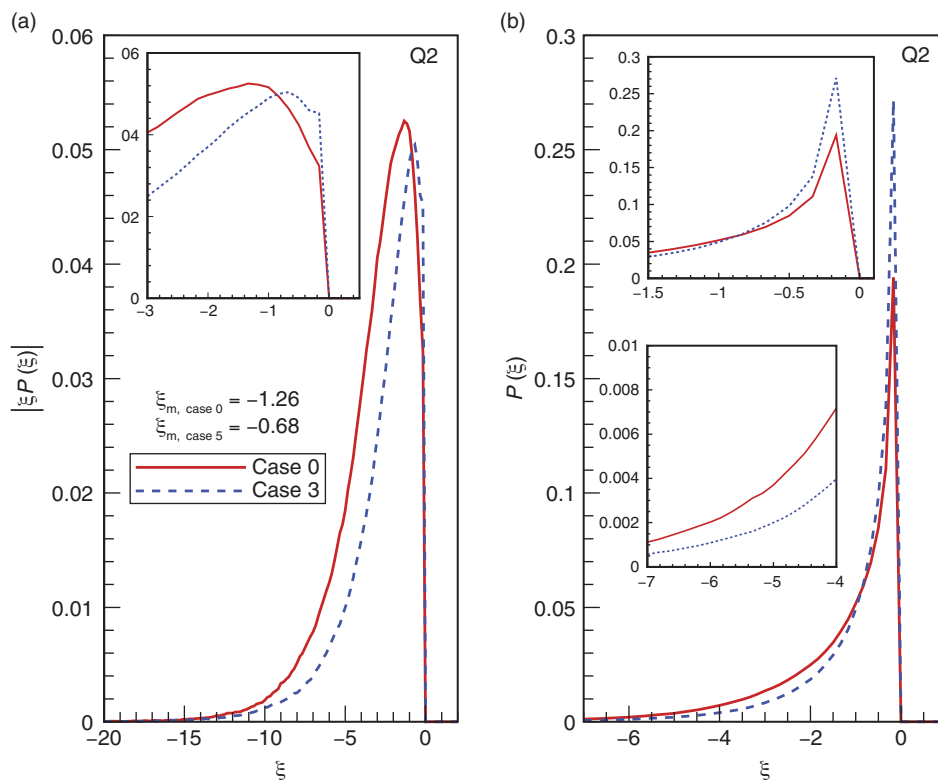

Figure 8. (a) Weighted probability density function of Q2 events. (b) Probability density function of Q2 events. The bed-normal location is $z^+ \sim 18$. The inset in (a) highlights the change in the maximizing Reynolds stress Q2 event form case 0 to case 3.

case 0 to case 3. However, the strength of the maximizing event ξ_m has decreased by 46%. More importantly, this decrease comes about by a 38 % reduction in the bed-normal velocity fluctuations. Thus, increase in settling velocity of sediments results in reorientation and damping of the Reynolds stress maximizing Q2 event vector. Similar observations can be made for the most likely Reynolds stress event (Q2 event that maximizes $P(\xi)$ see Figure 8(b)).

Zhou *et al*. (1999) considered conditionally averaged vortical structures in unstratified channel flow obtained for different levels of turbulent Reynolds stress events from $0.25^2\xi_m$ to $3.0^2\xi_m$.

They observed that the conditional vortical structure was able to auto-generate future generation of hairpin and quasi-longitudinal vortex structures when its intensity was greater than $2.0^2\xi_m$.

It is important to mention that the auto-generation criterion given by Zhou *et al*. (1999) was for unstratified single-phase channel flow and hence it cannot be directly extended to stratified multi-phase flows. As discussed above, the effect of increased settling velocity of sediments is not only to decrease ξ_m, but also to reorient the event vector $\tilde{u}'_m$ to be increasingly parallel to the bed. As the event vector flattens it is probable that even higher initial vortex strength will be required to spawn next generation of structures. Thus the threshold value is likely to be different and much greater than $2.0^2\xi_m$ for auto-generation in case of flows with suspended sediments. It can therefore be conjectured that when settling velocity of sediments is increased above the threshold, the change in the spatial structure of the vortical structures combined with the reduction in their strength, together preclude sustained regeneration of turbulent vortical structures and ultimately the flow loses all turbulence.

4.3 Turbulent structures and mechanistic view of complete turbulence suppression

Figures 9, 10 and 11 show iso-surfaces of swirling strength for cases 0, 3 and 4. Swirling strength has been shown to be very effective in extracting vortical regions in turbulent flows (Zhou *et al*. 1999; Chakraborty *et al*. 2005). In cases 0 and 3, the flow remains turbulent and thus the turbulent structures seen in Figures 9 and 10 are representative of what are seen at other times as well. Case 0 shows a dense and uniform distribution of hairpin-like and inclined quasi-streamwise vortices in the flow. Case 3 corresponds to the closest turbulent case to the critical settling velocity. At this near critical settling velocity, the stratification in the flow causes the structures to become sparse creating pockets in the flow completely devoid of vortical structures.
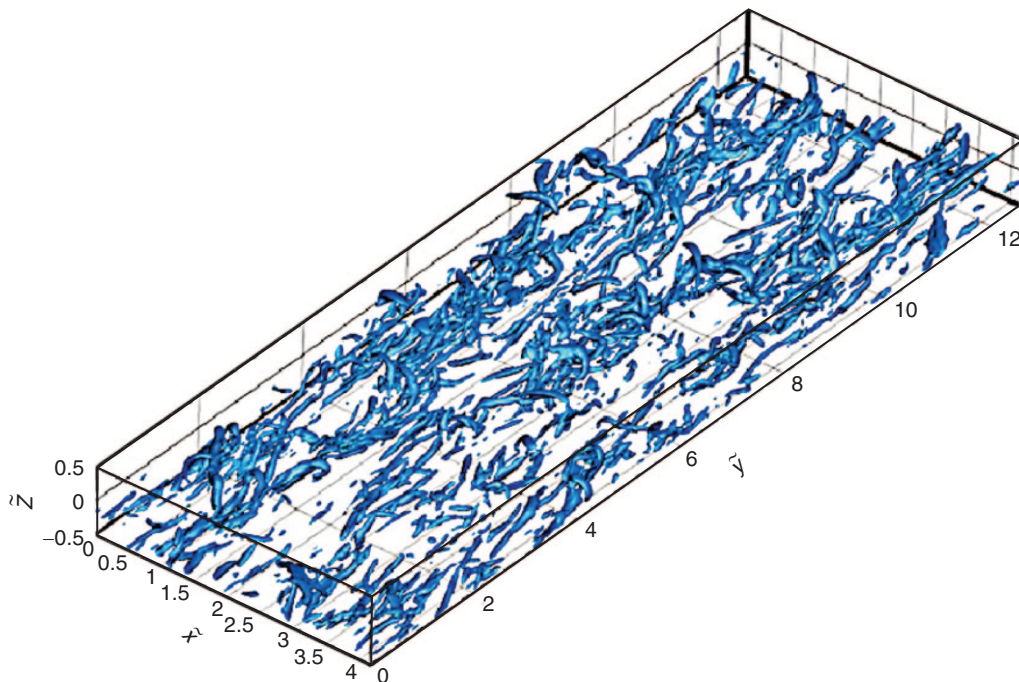
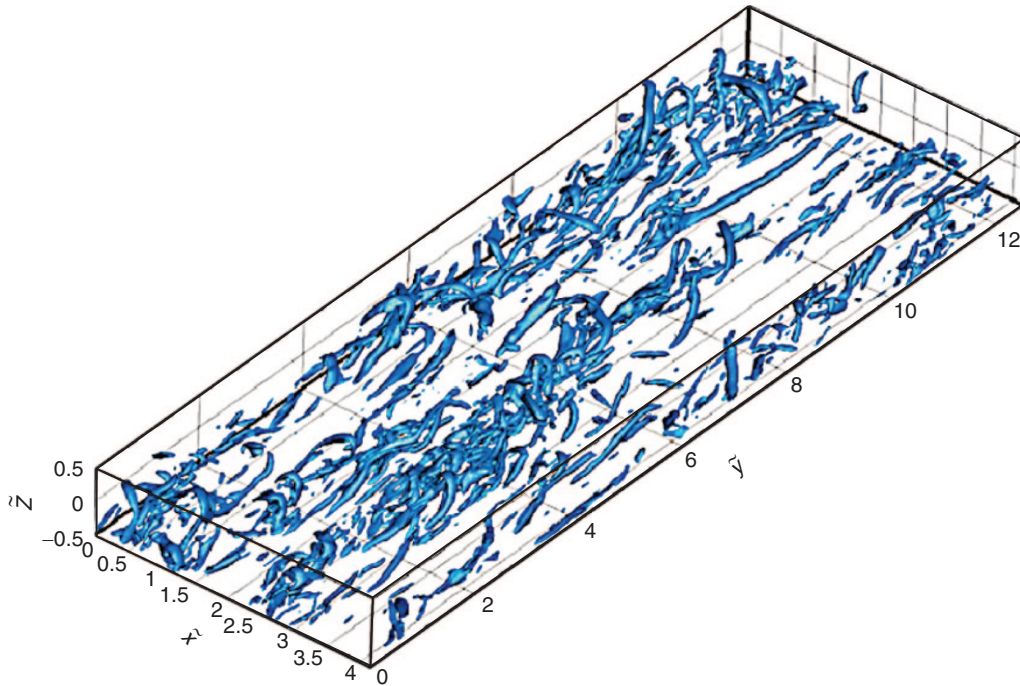

Figure 9. Iso-surfaces of λ_{ci} for case 0.

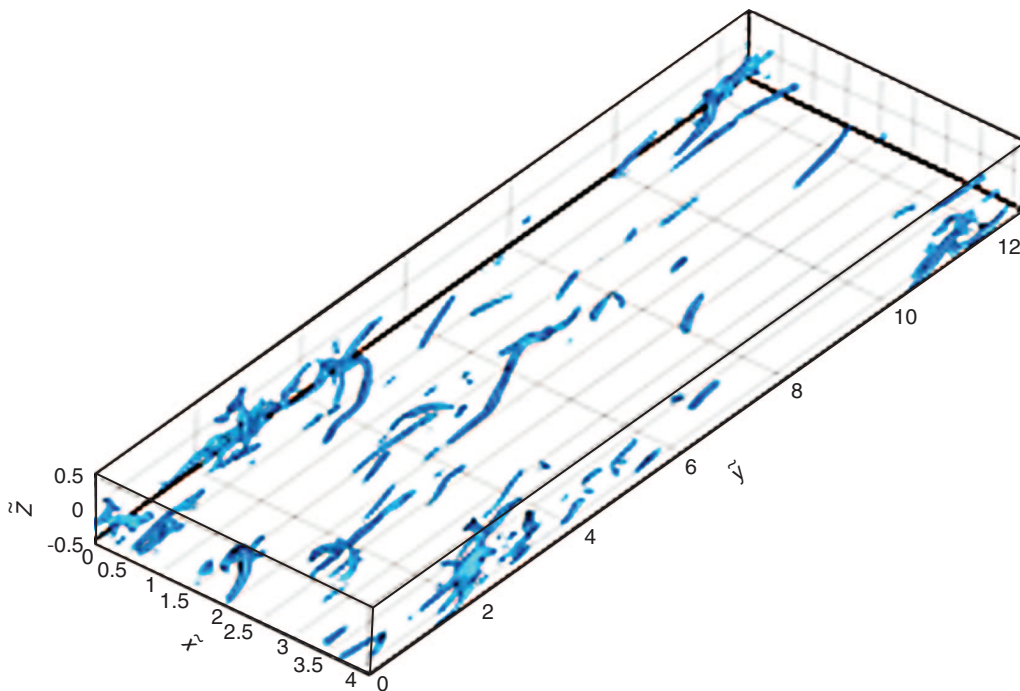Figure 10. Iso-surfaces of λ_{ci} for case 3.

Figure 11. Iso-surfaces of λ_{ci} for case 4. The iso-surfaces are $\lambda_{ci}=22$.

Since the flow in case 3 remains turbulent, it implies that some of the existing structures in the flow are intense enough to spawn next generation of structures to sustain turbulence. Case 4 corresponds to a settling velocity slightly above criticality and complete turbulence suppression is observed. Figure 11 shows the turbulent structures in case 4 at an instant when the flow is still in the process of turbulence suppression. Note that case 4 was started with a turbulent initial condition taken from case 3 and thus started with vortical structures similar to those shown in Figure 10.

However, due to the increased settling velocity, auto-generation process was disrupted and the flow has lost most of its turbulent structures. When continued, even the existing vortical structures in Figure 11 were not able to spawn the next generation of vortical structures and the flow lost all its turbulent fluctuations.

From the turbulent statistics and the picture of instantaneous turbulent structures the following simple scenario is proposed, which leads to seemingly sudden and abrupt loss of turbulence. In the limit of zero settling velocity, the sediments are perfectly well mixed at all times with zero concentration fluctuations. Here the turbulent wall layer is populated with streamwise aligned hairpin vortex packets (as discussed in Zhou *et al.* (1999)). These packets travel downstream and between their quasi-streamwise legs they cooperatively pump the near-bed low momentum fluid into the flow. These streaks provide an ideal environment for the subsequent formation of the next generation of hairpin packets. Figure 12 represents these streaks that are captured by the contour plots of Q2 events in the streamwise-spanwise plane close to the bed (this plane corresponds to $z^+ \sim 18$). The contour plots show that the streaks are uniformly distributed throughout the plane.

When we suddenly introduce sediments with non-zero settling velocity, the sediments are resuspended only in regions of sufficient upward (positive) bed-normal velocity fluctuations, while they settle down in regions of downward fluid motion. In particular, the streamwise aligned hairpin vortex packets provides the perfect environment for the upward transport of sediments. It is in these regions where increased sediment concentrations are expected. This process is captured in the contour plots shown in Figure 13a and 13b. Here we see that the contours of positive concentration fluctuations are well correlated with the contours of Q2 events. Thus, as the hairpin packets travel
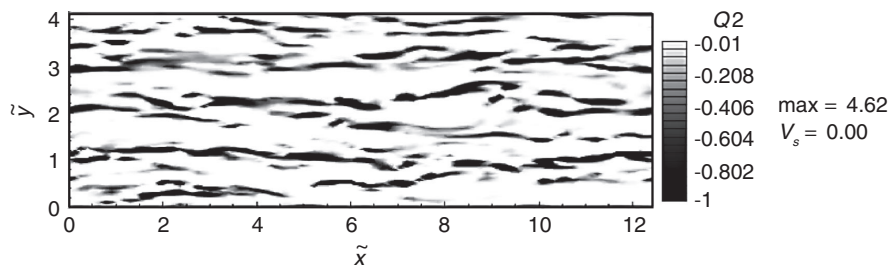

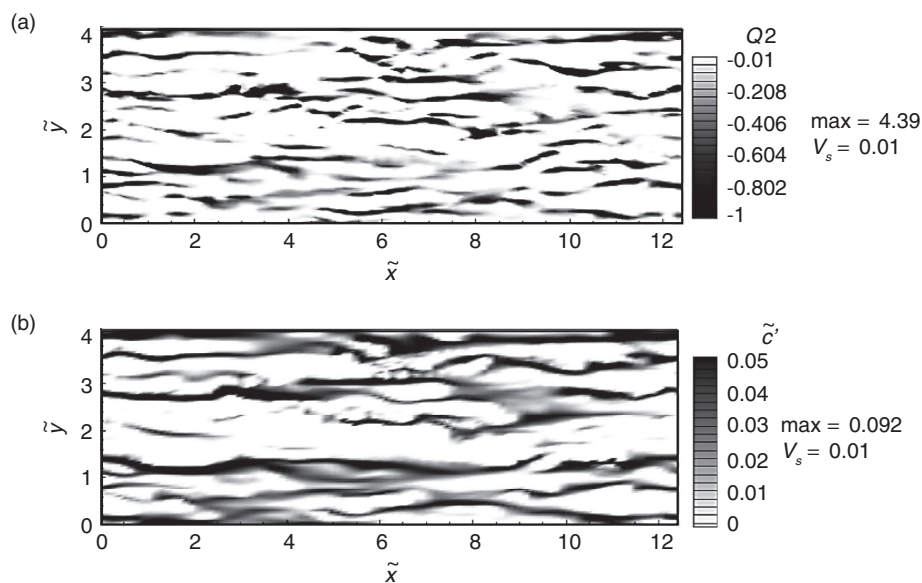Figure 12. Contour plots of Reynolds stress Q2 events at $z^+ \sim 18$ for case 0.

Figure 13. Contour plots of (a) Reynolds stress Q2 events and (b) concentration
fluctuations ($\tilde{c}'$) at $z^+ \sim 18$ for case 1.

downstream, similar to the long streaks of low speed fluid, they leave behind well-correlated long streaks of high sediment concentration. Thus, subsequent generation of hairpin vortices are being formed in regions of steadily increasing sediment concentration.

The increased concentration of sediment at the low speed streaks alters the character of the newly formed vortical structures. Furthermore, the additional buoyancy effect posed by the sediments can be expected to increase the threshold amplitude for the formation of next generation of vortical structures. Thus, increasing settling velocity of sediments leads to a decrease in the density of vortical structures. It can then be conjectured that once a threshold settling velocity is exceeded, the local accumulation of sediments at the low-speed streaks do not permit further generation of vortical structures. Without the auto-generation process active, the turbulence over time fully decays. Contour plots shown in Figure 13 and 14 are an indication of this mechanism. Figure 13 corresponds to case 1 where the sediment settling velocity is small and the stratification effect is weak. While Figure 14 corresponds to case 3 where the sediment settling velocity and the stratification effect is near critical. From case 0 to case 3, we see that the uniform distribution of Q2 events starts to breakdown and the Q2 events become less intense. The maximum Q2 event intensity encountered in the frame drops from 4.62 for case 0 to 3.64 for case 3. On the other hand, the concentration fluctuations increase explosively with increase in the settling velocity of the sediment particles. For case 3 large patches of high concentration fluctuations are observed and in these regions we see substantial reduction in the intensity of Q2 events. These observations suggest the possibility of the mechanistic proposal presented above.

4.4 Criteria for complete turbulence suppression

(20) can be integrated in bed-normal direction to give the global TKE balance. After integrating and applying the appropriate boundary condition, we get the following global TKE balance

$$\tilde{p} - \tilde{E} + \frac{1}{Re_\tau}\left\{\left[\frac{d\tilde{k}}{d\tilde{z}}\right]_0^1 + \frac{\zeta}{\tan\theta}\right\} = \beta + \mathrm{Ri}_\tau \tilde{V}_z, \qquad (21)$$

where,

$$\tilde{P} = \int_0^1 \tilde{P}\,d\tilde{z}, \quad \tilde{E} = \int_0^1 \tilde{\in}\,d\tilde{z}, \quad \beta = -\int_0^1 \overline{\tilde{w}'\tilde{c}'}\,d\tilde{z}, \quad \zeta = \frac{\overline{\tilde{c}}_b' - \overline{\tilde{c}}_t'}{Sc}.$$

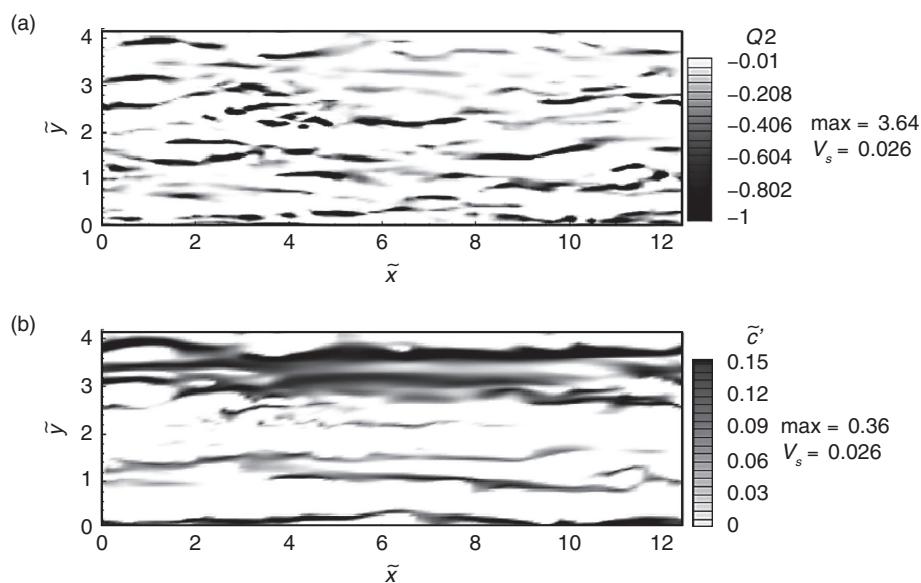

Figure 14. Contour plots of (a) Reynolds stress Q2 events and (b) concentration fluctuations ($\tilde{c}'$) at $z^+ \sim 18$ for case 3

Here $\bar{\tilde{c}}_b$ and $\bar{\tilde{c}}_t$ are the mean concentration on the bed and top boundary of the channel, respectively. Equation (21) represents the global TKE balance. The TKE spent to maintain sediments in suspension is captured by the two terms on the right hand side of (21). When enough TKE is not available to maintain the sediments in suspension, net sedimentation will occur and the flow extinguishes eventually.

Here we propose that $Ri_\tau \widetilde{V}_z$ represents the total TKE spent to keep sediments in suspension (since $\tilde{\beta}$ is observed to be a fraction of $Ri_\tau \widetilde{V}_z$ in all the cases considered). Therefore, the condition for turbulence suppression is $Ri_\tau \widetilde{V}_z > K_c$, where K_c is the critical value beyond which suspended sediments completely extinguish turbulence.

We have observed from previous figures that show various turbulence statistics that as long as the flow remains turbulent, turbulence statistics shows only a weak dependence on $\widetilde{V}_z$. Therefore to understand the effect of Reynolds number on the critical value K_c, we seek the Re_τ dependence of TKE in a pure turbulent channel flow without sediments. In this limit TKE production can be exactly expressed as (Zanoun *et al*. 2009):

$$\tilde{P} = Re_\tau \left(g(\tilde{z}) - \tilde{z} \right) \left(1 - g(\tilde{z}) \right) \; where \; g(\tilde{z}) = -\overline{\tilde{u}'\tilde{w}'} + \tilde{z}.$$

To obtain an estimate of TKE production, we use the empirical function proposed by Panton 2007,

$$g(\tilde{z}) = \frac{2}{\pi} \arctan \left(\frac{0.82 \, Re_\tau \tilde{z}}{\pi} \right) \left[1 - \exp \left(-\frac{Re_\tau \tilde{z}}{7.8} \right) \right]^2 \qquad (22)$$

Integrating the TKE production expression using the above empirical function gives a scaling relation for global TKE production with the Reynolds number. This scaling can be written as $\widetilde{P} \approx 2.46 \ln(Re_\tau) - 5.97$. This means that it is quite likely that K_c will also have logarithmic dependence on Re_τ. We use laboratory and field data to validate this hypothesis. More details on the laboratory and field data can be found in our recent work Cantero *et al*. (2012b). It must be recognized, however, that the field observations and laboratory experiments were not conducted with the goal of establishing the threshold value of K_c. As a result, some of the information needed in the calculation of K_c was not measured or reported, in which case we estimate a plausible range of values and compute the corresponding range of K_c. Figure 15 presents the values of K_c obtained from various experimental and field observations and are plotted against Re_τ. This figure
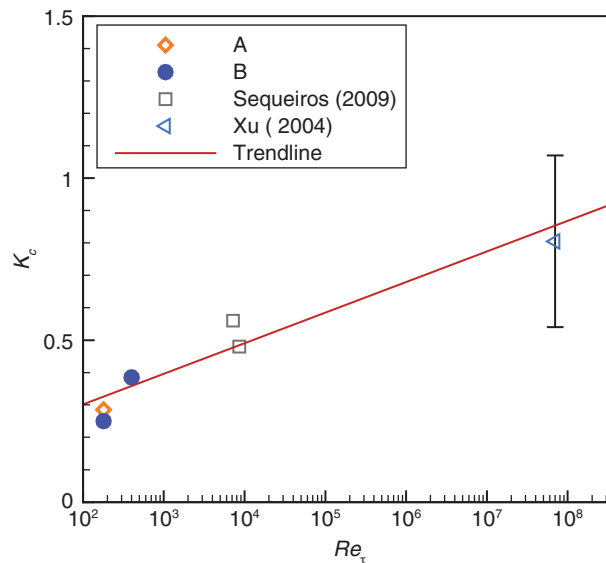

Figure 15. Evolution of K_c with Re_τ. Data points are obtained from our DNS cases, experiments and field observations. For complete details on the experiments and field measurements refer to Cantero et al., (2012b).

also includes the simulation results for $Re_\tau = 180$ and 400. The best fit is $Ri_\tau \widetilde{V}_z\big|_{crit} = K_c(Re_\tau) \approx$ $0.041\ln(Re_\tau) + 0.11$. The experimental and field data show a definite upward trend, but exhibit considerable scatter. Thus, the scaling for K_c is only intended to be a guideline. Clearly, additional higher Re_τ simulations and experiments with a focus on observing turbulence suppression by stratification are needed.

4.5 Bi-disperse suspensions

Now that we have a better understanding of the mechanisms of total turbulence suppression in turbidity currents driven by mono-disperse sediment suspensions, and that we have provided a criterion for predicting total turbulence suppression in mono-disperse turbidity currents, it will be interesting to extend and validate these findings for bi-disperse turbidity currents.

We consider different suspensions in 2 sets A and B. In sets A and B the settling velocity of coarse sediments is fixed at 0.0275 and 0.035, respectively and the proportion of coarse to fine sediments is varied. In each set we start with a suspension containing a lot of fine sediments ($\gamma_f = 1$), which keeps the stratification effects to minimum. In subsequent cases (suspensions), the quantity of coarse sediments is increased at the expense of fine sediments. Thus, we increase the stratification effect in the flow while keeping the total sediment load constant. Eventually a critical suspension composition is reached so that even a small increase in the amount of coarse sediments will result in complete turbulence suppression. The critical suspension composition lies between cases 3B and 4B for set B. In set A, the critical composition is somewhere between case 3A and the extreme case of no fine sediments in the flow, i.e., $\gamma_f = 0$. From the mono-disperse simulations shown previously we know that $\gamma_f = 0$ for $\widetilde{V}_c = 0.0275$ will result in complete turbulence suppression. Complete details of all the simulations are listed in Table 2.

Here we will consider some of the cases from set B and analyse the associated turbulence statistics for statistically steady flow. This analysis is intended to show the effect of composition of the bi-disperse suspension on the flow and the existence of critical composition, which brings about complete turbulence suppression. Figure 16(a) and 16(b) presents the mean sediment concentration ($\overline{\widetilde{c}}_c + \gamma_f$) and mean streamwise velocity ($\overline{\widetilde{u}}$) profiles in the bed-normal direction for cases 1B, 2B, 3B, 4B and $\gamma_f = 1$. $\gamma_f = 1$ implies turbidity current driven by uniform body force (or mono-disperse suspension of sediments with zero settling velocity, see case 0 from Shringarpure et al., (2012)) and is used as a reference to compare the
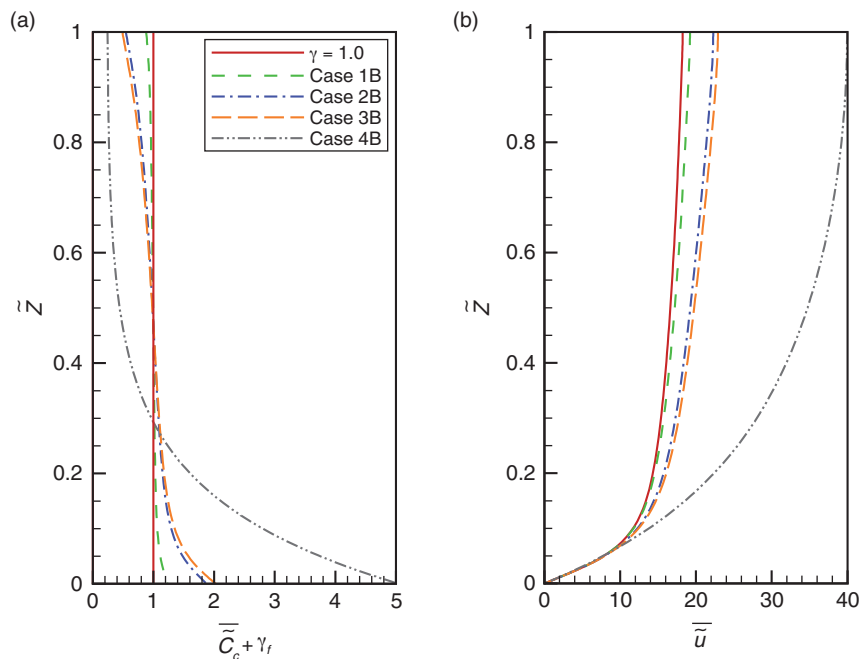

Figure 16. (a) Combined mean sediment concentration. (b) Mean velocity profiles. Refer to Table 2 for complete details of the cases shown in the figures.

stratification effects of different bi-disperse suspensions. From case 1B to 4B the amount of coarse sediment particles increases, thus increasing the stratification imposed on the flow. This increasing trend is seen in Figure 16(a). The mean sediment concentration at the bed increases from 1.232 for case 1B to 5.036 for case 4B. Similarly the concentration gradient near the bed is seen to increase for case 1B to case 4B. Observe that from case 3B to case 4B there is a sudden change in the mean concentration profile that can be attributed to redistribution of coarse sediments in the channel. Most of the sediments are now concentrated close to the bed indicating loss in the mixing ability of the flow.

Mean velocity profiles tell a similar story. From case 1B to 4B as the stratification increases, it inhibits vertical exchange of momentum and as a consequence the mean streamwise velocity gradient and the maximum mean streamwise velocity increases in the channel. This leads to increase in the bulk streamwise velocity (can also be interpreted as average mean velocity or flow rate) in the channel. Similar to mean concentration profiles, a substantial change in $\bar{\tilde{u}}$ profiles is seen from case 3B to 4B. There is an abrupt jump in the bulk velocity and maximum streamwise velocity from case 3B to case 4B.

Figure 17(a) presents the Reynolds stress $\overline{\tilde{u}'\tilde{w}'}$ profiles for different cases from set B. Reynolds stress modulations are a representation of the stratification effect on the flow. The profiles show slight damping as γ_f decreases from 0.75 for case 1B to 0.24 for case 3B. Beyond case 3B, even with a slight decrease in $\gamma_f = 0.235$ (case 4B) there is abrupt and complete suppression of Reynolds stress. Figure 17(b) shows the profiles of ratio of Reynolds flux $\overline{\tilde{w}'\tilde{c}'}$ to settling flux $\tilde{V}_z\bar{\tilde{c}}$ for different cases from set B. Reynolds flux is a measure of turbulent mixing in the bed-normal direction. Thus the ratio of Reynolds flux to settling flux represents the bed-normal mixing ability of the flow. Similar to Reynolds stress profiles, we can observe that from case 1B to case 3B only slight damping is seen in the mixing ability of the flow. But, beyond case 3B there is abrupt and total suppression of turbulent mixing $\overline{\tilde{w}'\tilde{c}'}$ leading to complete loss in the mixing ability of the flow.

In summary, the above turbulence statistics reveal that complete turbulence suppression occurs when γ_f is reduced from 0.24 to 0.235. An interpretation of the above results would imply that at $Re_\tau = 180$ and slope $\theta = 5°$, to transport sediments with settling velocity of 0.035 in bi-disperse suspension, the fine sediments ($\tilde{V}_f = 0.0$) need to make up at least 24% of the total sediment load. Similar observations can be made from the other set A.
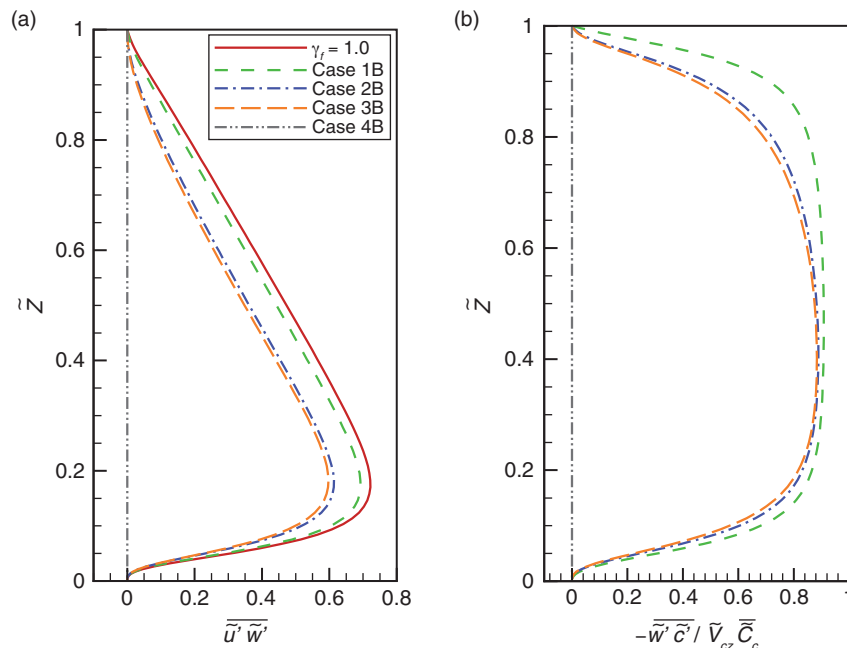

Figure 17. (a) Reynolds stress profiles. (b) Profiles of ratio of Reynolds flux to settling flux of sediments. Refer to Table 3 for the details of all the cases shown in the figures.

4.6. Mechanism of total turbulence suppression in Bi-disperse suspensions

In section 4.3, we identified a possible mechanism by which total turbulence suppression occurs in turbidity currents driven by mono-disperse suspension of sediments. This mechanism proposes that settling sediments shuts down the auto-generation process of the near wall hairpin and quasi-streamwise structures which is essential in sustaining turbulence in the flow. The accumulation of sediments greatly alters the structures, i.e., their intensity is damped and their shape is modulated. The shutdown in the auto-generation process is brought about by excessive accumulation of sediment particles in the region of low speed streaks. The point of excessive accumulation is reached at the critical sediment settling velocity. How good is this mechanistic viewpoint for turbulence suppression in turbidity currents driven by bi-disperse suspensions.

Figure 18(a) and 18(b) shows the contour plot of Q2 events and concentration fluctuations for case 1B in a streamwise-spanwise plane close to the bottom wall. As expected the Q2 events are nearly uniformly distributed throughout the plane as the suspension is mostly comprised of fine sediment particles. Also, we see good correlation between the positive concentration fluctuation and the Q2 events in the flow. From case 1B to case 3B, the amount of coarse sediment particles increases at the expense of fine, i.e., the stratification effect in the flow increases. In figure 19(a) and 19(b), which shows the contour plots of Q2 events and concentration fluctuations for case 3B, we see that the Q2 event are not nearly as uniform as case 1B or case 0 in Figure 12. Furthermore, the maximum Q2 event intensity encountered in the frame has also reduced (from 6.08 for case 1B to 3.79 for case 3B). Substantial increase in the concentration fluctuations is also seen for case 3B. These figures are qualitatively very much similar to Figures 12, 13 and 14 that show the contour plots for mono-disperse suspensions. Based on these observations, it implies that the mechanism of turbulence suppression in turbidity currents driven by bi-disperse and mono-disperse suspensions is similar.

4.6 Turbulence suppression criteria for Bi-disperse suspensions

TKE equation of turbidity currents driven by bi-disperse suspensions can be written as

$$\tilde{P} - \tilde{\mathcal{E}} - \frac{d}{d\tilde{z}}\left[\overline{\tilde{w}'\tilde{p}'} + \overline{\tilde{k}\tilde{w}'} + \frac{1}{Re_\tau}\frac{d\tilde{k}}{d\tilde{z}} \right] = -\overline{\tilde{u}'\tilde{c}_c'} + \text{Ri}_\tau\,\overline{\tilde{w}'\tilde{c}_c'}. \qquad (23)$$

All the terms in the above equation have their usual meaning. Notice that only those terms that contain coarse sediment concentration remain on the right hand side. As before, equation (23) can be intergrated in wall normal direction to give the total TKE budget.
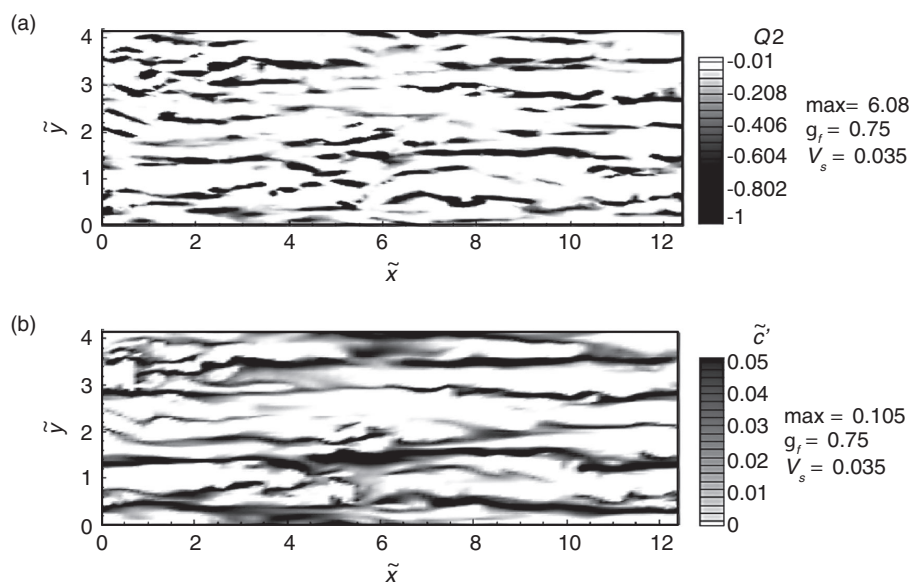

Figure 18. Contour plots of (a) Q2 events and (b) ($\tilde{c}'$) at $z^+ \sim 18$ for case 1B.
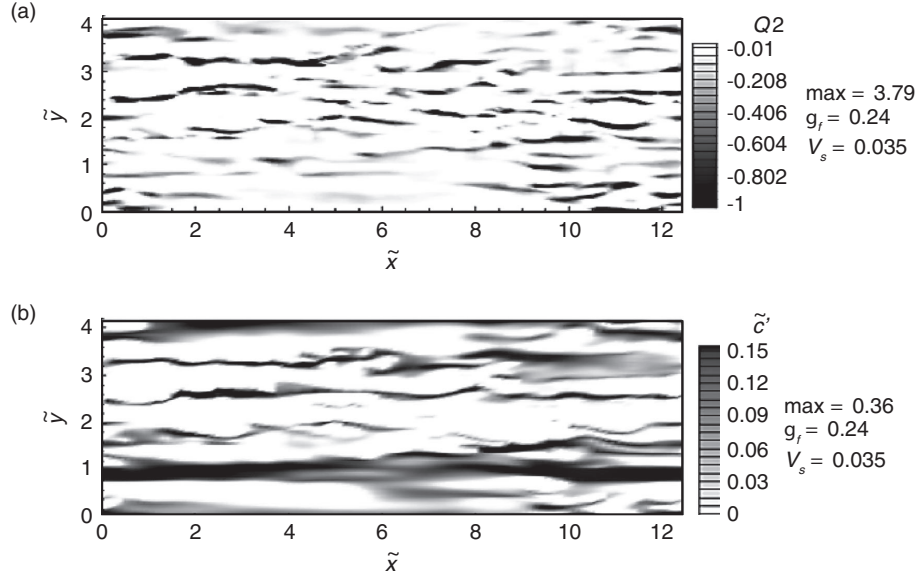
Figure 19. Contour plots of (a) Reynolds stress Q2 events and (b) concentration
fluctuations ($\tilde{c}'$) at $z^+ \sim 18$ for case 3B.

**Table 3. Turbulent kinetic energy balance of near critical cases from sets A and B. Also
included in the table is the TKE balance of the near critical case of mono-disperse
suspension.**

Case	$\tilde{V}_{cs}$	γ_f	$\tilde{P}$	$\tilde{\in}$	β_c	$Ri_\tau \gamma_c \tilde{V}_{cz}$	$Ri_\tau \zeta_c /Re_\tau$	$\gamma_c \tilde{V}_{sc}$
3A	0.0275	0.04	6.534	6.179	0.113	0.302	0.0978	0.0264
3B	0.035	0.24	6.598	6.237	0.117	0.304	0.0977	0.0266
3	0.026	1.0	6.590	6.230	0.117	0.296	0.0958	0.0260

$$\tilde{P} - \tilde{E} + \frac{1}{Re_t}\left\{\left[\frac{d\tilde{k}}{d\tilde{z}}\right]_0^1 + \frac{\zeta_C}{\tan\theta}\right\} = \beta_C + Ri_\tau \gamma_C \tilde{V}_Z \,,$$

(24)

where

$$\tilde{p} = \int_0^1 \tilde{p}\,d\tilde{z}, \quad \tilde{E} = \int_0^1 \tilde{\in} d\tilde{z}, \quad \beta_c = -\int_0^1 \overline{\tilde{W}'\tilde{C}_c'}\,d\tilde{z}, \quad \zeta_c = \frac{\overline{\tilde{C}}_{cb} - \overline{\tilde{C}}_{ct}}{Sc}.$$

As expected the turbulence damping effects (terms on the right hand side of (23), (24) are only due to the coarse sediments. This means that in such type of bi-disperse suspensions where the size of coarse sediments is fixed, the fractional volume concentration of coarse sediments, i.e. γ_c, controls complete turbulence suppression in the flow. Table 3 presents the TKE budget for cases that are closest to the critical turbulence-damping limit for the sets A and B. The TKE budget of case 5 which is the case closet to the critical turbulence damping limit for currents with mono disperse suspension of sediment, is also given in Table 3. The TKE budget for these cases shows a striking agreement. As the critical state is approached the bulk TKE production ($\tilde{P}$) and TKE dissipation ($\tilde{\in}$) in the channel are observed to be insensitive to the composition of the suspension. Similarly, the damping terms β_c and $Ri_\tau \tilde{V}_{cz}\gamma_c$ for the bi-disperse cases (3 and 3B) and the corresponding damping terms for the mono disperse case 3 from Table 1 are in close agreement.

5. CONCLUSIONS

We have modeled dilute turbidity currents in bypass mode as an inclined channel flow driven by mono-disperse and bi-disperse suspensions of sediments. These suspended sediments under the influence of gravity drive the flow and simultaneously settle towards the bed. The interaction of sediments and turbulence leads to: (a) skewing of the streamwise driving force towards the bed and (b) stable stratification that damps bed-normal momentum and mass transport. We have carried out several simulations of turbidity currents driven by mono-disperse suspensions to understand the interaction of settling sediments and flow turbulence. We observe that at high enough sediment settling velocity, the strong stratification is responsible for completely suppressing turbulence in the flow. For the mono-disperse simulations with $Re_\tau = 180$ and $\theta = 5°$, the critical settling velocity lies between case 3 ($\widetilde{V}_z = 0.026$) and case 4 ($\widetilde{V}_z = 0.0265$). This means that the flow can be divided into two regimes, i.e. turbulence-stratified flows and turbulence-suppressed flows. Furthermore, there is sudden transition from one regime to another at the critical sediment settling velocity value.

For mono-disperse simulations three parameters: Re_τ, Ri_τ and $\widetilde{V}_z$ are identified that characterize the abrupt turbulence suppression in the flow. From TKE equation the parametric grouping $Ri_\tau \widetilde{V}_z$ is obtained, which represents the energy spent to keep sediments in suspension. We have shown that a critical value of $Ri_\tau \widetilde{V}_z$ exist beyond which turbulence is completely extinguished by stratification. Furthermore, from the scaling relations of TKE production and TKE dissipation with Re_τ in a pure channel flow, we propose a logarithmic dependence for critical $Ri_\tau \widetilde{V}_z$ with increasing Re_τ.

We have also carried out several simulations of turbidity currents driven by bi-disperse suspensions. These simulations are carried out at the same Re_τ and Ri_τ as the mono-disperse simulations. This facilitates the comparison of turbulence suppression mechanisms and the criteria for complete turbulence suppression presented for the mono-disperse simulations with the bi-disperse simualtions. In the bi-disperse model, fine sediments are assumed to have negligible settling velocity and hence they maintain nearly uniform concentration throughout the channel. On the other hand, the coarse sediments are such that they have large settling velocity and impose a strong turbulence damping effect on the flow. Therefore the asymptotic state of the flow is determined by the combined effect of these two sediment types. Various simulations were carried out under two sets A and B, where sets A and B correspond to coarse sediments with settling velocity 0.0275 and 0.035, respectively. In the two sets, there exist as critical composition (fine to coarse sediment proportion) such that even a small increase in the amount of coarse sediments (at the expense of fine sediments) leads to complete turbulence suppression. This sudden turbulence suppression is very much similar to the trends observed in the mono-disperse simulations, i.e. in subcritical suspension composition the flow remains vigorously turbulent with slight damping in its intensity, but as soon as the critical composition is reached it brings about complete turbulence suppression. Through simulations it is evident that a minimum quantity of fine sediments is needed to keep the flow alive i.e. to keep turbulence active so that the coarse sediments can be retained in suspension. This is the underlying mechanism by which real turbidity currents derive their ability to transport large/heavy sediments for long distances.

Turbulence suppression mechanism is first explored for currents carrying mono-disperse suspension of sediments. It is proposed that the turbulence suppression occurs because the turbulent structures existing in the flow become incapable of spawning subsequent generation of vortical structures. Zhou et.al. 1999 have shown that turbulent structures of sufficiently strong intensity possess the ability of auto-generation. Through statistical analysis of Q2 events and visualization of vortical structures close to the wall, we identified that settling sediment lead to local regions of high positive concentration fluctuations which occur near the Q2 events (low speed streaks). This accumulation damps the intensity of structures and modulates their shape. The global effect of this is that the flow looses energetic structures that are capable of auto-generation and in time all the turbulence dissipates. The simulation of bi-disperse suspensions shows that this viewpoint is robust and similar observations can be made even for bi-disperse suspensions.

ACKNOWLEDGEMENTS

REFERENCES

[1]   Adrian, R. J. Stochastic estimation of conditional structure: a review. *Applied Scientific Research,* 53, 291–303, (1994).

[2]   Adrian, R. J. Hairpin vortex organization in wall turbulence. *Physics of Fluids* 19 (4), 041301, (2007).

[3]   Allen, J. R. L. Principles of Physical Sedimentology. The Blackburn Press, (2001).

[4]   Bernard, P. S., Thomas, J. M. & Handler, R. A. Vortex dynamics and production of Reynolds stress. *J. Fluid Mech*. 253, 385–419, (1993).

[5]   Brooke, J. W. & Hanratty, T. J. Origin of turbulence-producing eddies in a channel flow. *Physics of Fluids* 5, 1011–1022, (1993).

[6]   Bonometti, T. & Balachandar, S. Effect of schmidt number on the structure and propagation of density currents. *Theo. and Comp. Fluid Dynamics*, 22, 341–361, (2008).

[7]   Cantero, M. I., Balachandar, S., Cantelli, A., Pirmez, C. & Parker, G. Turbidity current with a roof: Direct numerical simulation of self-stratified turbulent channel flow driven by suspended sediment. *J. Geophys. Res*. 114, (2009a).

[8]   Cantero, M. I., Balachandar, S. & Parker, G. Direct numerical simulation of stratification effects in a sediment-laden turbulent channel flow. *J. Turbulence* 10, 1–28, (2009b).

[9]   Cantero, M. I., Balachandar, S. & Garcıa, M. H. An Eulerian Eulerian model for gravity currents driven by inertial particles. *International Journal of Multiphase Flow* 34, 484–501, (2008a).

[10]   Cantero, M. I., Balachandar, S., Garc´ıa, M. H. & Bock, D. Turbulent structures in planar gravity currents and their influence of the flow dynamics. *J. Geophy. Res*. 113, (2008b)

[11]   Cantero, M. I., Cantelli, A., Pirmez, C., Balachandar, S., Mohrig, D., Hickson, T. A., Yeh, T., Naruse, H. & Parker, G. Emplacement of massive turbidites linked to extinction of turbulence in turbidity currents. *Nature Geosci*. 5 (1), 42–45, (2012a).

[12]   Cantero, M. I., Garc´ıa, M. H. & Balachandar, S. Effect of particle inertia on the dynamics of depositional particulate density currents. *Computers and Geosciences* 34, 1307–1318, (2008c)

[13]   Cantero, Mariano I., Shringarpure, Mrugesh & Balachandar, S. Towards a universal criterion for turbulence suppression in dilute turbidity currents with non-cohesive sediments. *Geophys. Res. Lett*. 39 (14), (2012b).

[]14   Canuto, C., Hussaini, M., Quarteroni, A. & Zang, T. Spectral methods in Fluid Dynamics. New York: Springer, (2012).

[15]   Chakraborty, P., Balachandar, S. & Adrian, R. J. 2005 On the relationships between local vortex identification schemes. *J. Fluid Mech*. 535, 189–214.

[16]   Cortese, T. A. & Balachandar, S. High performance spectral simulation of turbulent flows in massively parallel machines with distributed memory. International Journal of High Performance Computing Applications 9, 187–204, (1995).

[17]   Ferry, J. & Balachandar, S. A fast Eulerian method for disperse two-phase flow. *International Journal of Multiphase Flow* 27, 1199–1226, (2001).

[18]   Garcia, M. H. & Parker, G. Experiments on the entrainment of sediment into suspension by a dense bottom current. *J. Geophys. Res*. 98, 4793–4807, (1993).

[19]   Krause, D. C., White, W. C., Piper, D. J. W. & Heezen, B. C. Turbidity currents and cable breaks in the western New Britain trench. *Geological Society of America* Bulletin 81, 2153–2160, (1970).

[20]   Laadhari, F., On the evolution of maximum turbulent kinetic energy production in a channel flow, *Phys. Fluids,* 14 (10), L65–L68, (2002).

[21]   Laadhari, F., Reynolds number effect on the dissipation function in wall-bounded flows, *Phys. Fluids,* 19 (3), (2007).

[22]   Mucha, P. J. & Brenner, M. P. Diffusivities and front propagation in sedi-mentation. *Phys. Fluids*, 15 (5), 1305–1313, (2003).

[23]   Necker, F., Hartel, C., Kleiser, L. & Meiburg, E. Mixing and dissipation in particle-driven gravity currents. *J. Fluid Mech*. 545, 339–372, (205).

[24]   Pantin, H. M. Interaction between velocity and effective density in turbidity flow: Phase-plane analysis, with criteria for autosuspension. *Marine Geology* 31 (1–2), 59–99, (1979).

[25]   Panton, R. L., Composite asymptotic expansions and scaling wall turbulence, *Phil. Trans. Roy. Soc. A-Mathematical Physical and Engineering Sciences*, 365 (1852), 733–754, (2007).

[26]   Parker, G. Conditions for the ignition of catastrophically erosive turbidity currents. *Marine Geology* 46, 307–327, (1982).

[27]   Parker, G. In Sedimentation Engineering: Processes, Measurements, Modeling and Practice (ed. M. H. Garcia), pp. 165–252. ASCE, (2008).

[28]   Pinet, P. R. Invitation to oceanography, 4th edn. Jones and Bartlett, (2006).

[29]   Pirmez, C. & Imran, J. Reconstruction of turbidity currents in Amazon Channel. *Marine and Petroleum Geology* 20, 823–849. (2003).

[30]   Segre, P. N., Liu, F., Umbanhowar, P. & Weitz, D. A. An effective gravitational temperature for sedimentation. *Nature* 409, 594–597. (2001).

[31]   Sequeiros, O. E., H. Naruse, N. Endo, M. H. Garcia, and G. Parker, Experimental study on self-accelerating turbidity currents, *J. Geophys. Res.*, 114, (2009).

[32]   Shringarpure, Mrugesh, Cantero, Mariano I. & Balachandar, S. Dynamics of complete turbulence suppression in turbidity currents driven by monodisperse suspensions of sediment. *Journal of Fluid Mechanics*, 712, 384–417, (2012).

[33]   Simpson, J. E. Gravity currents: In the environment and the laboratory, 2nd edn. Cambridge university press, (1997).

[34]   Sumner, E. J., P. J. Talling, and L. A. Amy, Deposits of flows transitional between turbidity current and debris flow, *Geology*, 37(11), 991–994, (2009).

[35]   Talling, P. J., et al., Onset of submarine debris flow deposition far from original giant landslide, *Nature*, 450 (7169), 541–544, (2007).

[36]   Xu, J. P., M. A. Noble, and L. K. Rosenfeld, In-situ measurements of velocity structure within turbidity currents, *Geophys. Res. Letters*, 31(9), (2004).

[37]   Zanoun, E., and F. Durst, Turbulent momentum transport and kinetic energy production in plane-channel flows, *Int. J. Heat and Mass Transfer*, 52, 4117–4124, (2009).

[38]   Zhou, J, Adrian, R. J. & Balachandar, S. Autogeneration of near-wall vortical structures in channel flow. *Physics of Fluids* 8, 288–290, (1996).

[39]   Zhou, J., Adrian, R. J., Balachandar, S. & Kendall, T. M. Mechanisms for generating coherent packets of hairpin vortices in channel flow. *J. Fluid Mech.* 387, 353–396, (1999)